Macromolecules

ARTICLE

pubs.acs.org/Macromolecules

Intrinsically Microporous Poly(imide)s: Structure−Porosity Relationship Studied by Gas Sorption and X-ray Scattering

Nicola Ritter,[†] Irena Senkovska,[‡] Stefan Kaskel,[‡] and Jens Weber*[,†]

[†]Department of Colloid Chemistry, Max-Planck-Institute of Colloids and Interfaces, Science Park Golm, D-14424, Potsdam, Germany

[‡]Department of Inorganic Chemistry, Dresden University of Technology, Bergstr. 66, D-01069 Dresden, Germany

Supporting Information

ABSTRACT: Intrinsically microporous soluble poly(imide)s were prepared via polycondensation from (±)-2,2′-diamino-1,1′-binaphthalene or 4,4′-(9-fluorenylidene)dianiline and four different linear comonomers: pyromellitic dianhydride, 3,3′,4,4′-biphenyltetracarboxylic dianhydride, 4,4′-oxidiphthalic anhydride, and 4,4′-(hexafluoroisopropylidene)diphthalic anhydride. The porosity of the resulting eight poly(imide)s was determined by nitrogen, argon, hydrogen, and carbon dioxide sorption for precipitated and cast samples and compared. While only the stiffest and most porous poly(imide)s were able to adsorb nitrogen and argon, almost all polymers were able to adsorb hydrogen and carbon dioxide. On the basis of the sorption results, it was possible to determine the limit of intrinsic microporosity. The processing of the polymers has a major influence on the porosity as investigated by gas sorption and X-ray scattering. Solvent cast films are denser and can therefore be regarded as thermodynamically stable. Interestingly, we observed selective gas sorption phenomena (high carbon dioxide sorption but low hydrogen sorption) for some of the polymers. Finally, we investigated the response of one poly(imide) thin film to changing gas atmosphere by ellipsometry.

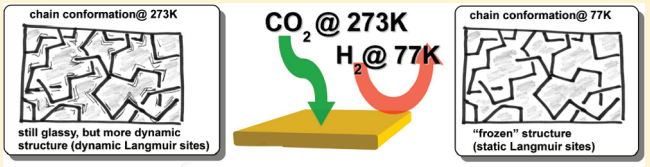

INTRODUCTION

Microporous, purely organic materials gained increasing interest during the past years as they have a high potential in a variety of applications like gas separation and storage or as catalyst (support) materials.[1−3] Because of recent synthetic advances, there is a broad structural variety of cross-linked microporous polymers available, as there are for instance poly(benzodioxane)s,[2,4−6] poly(imide)s,[7,8] poly(aniline)s,[9] various conjugated polymers,[3,10−14] poly(organosilanes),[15,16] poly(arylcarbinols),[17,18] and various hyper-cross-linked polymers.[19−24] This pool of polymer architectures is complemented by regular frameworks, covalent organic frameworks that are based on boron−oxygen, imine, or triazine systems.[25−30]

On the other hand, there is a great interest in soluble, microporous polymers (which are consequently not cross-linked), as they are much easier to process. However, only a very limited number of microporous, soluble polymers are known up to now. This can be related to the high demands which are posed onto polymer architecture in order to provide both high free volume and resistance against pore collaps. The most prominent examples of soluble microporous polymers are the polymers of intrinsic microporosity (PIM)s.[31−36] They feature a 90° kink in every repeat unit of the otherwise stiff ladder-type poly(benzodioxane)s. This kink prohibits the space-efficient packing of the polymer chains and lead to a large, interconnected amount of free volume. This free volume is accessible to probe molecules, as for instance nitrogen, and the polymers are therefore considered to be microporous. In former communications, we showed that the principle can be expanded on soluble poly(imide) using spirobifluorene or binaphthalene as the building block.[37,38] Furthermore, Ghanem et al. presented microporous, soluble poly(imide)s based on the classic PIM motif.[39] These microporous poly(imide)s might also be regarded as a continuation of the *cardo* concept, which was proposed already long time ago.[40]

It is the aim of the present study to investigate the influence of the molecular structure on the observable porosity in greater detail. While the influence of intermolecular interactions on the observable porosity was investigated in another study,[41] this study focuses on the impact of polymer backbone architecture (kink angle, monomer length, stiffness, etc.) We use ±1,1′-diamino-2,2′-binaphthalene (BINAM) and 4,4′-(9-fluorenylidene)dianiline (FDA) as stiff, kinked monomers. The two monomers feature different kink angles of ∼78° and ∼109°, respectively. Condensation of these monomers with various dianhydride comonomers allows a tuning of the overall polymer flexibility and the spacing between the kinks along the polymer chain.

The porosity of the samples will be analyzed by means of gas sorption, employing nitrogen, argon, hydrogen, and carbon dioxide as probe molecules. X-ray scattering will be used as a further tool to analyze the polymer microstructure.

EXPERIMENTAL PART

Materials. ±2,2′-Diamino-1,1′-binaphthalene (98% Aldrich), 99% ABCR, 4,4′-(9-fluorenylidene)dianiline (99% Aldrich), benzene-1,2,4,5-

Received: October 27, 2010
Revised: February 3, 2011
Published: February 28, 2011

tetracarboxylic dianhydride (99%, Acros) (recrystallized from acetic acid anhydride), 4,4′-oxidiphthalicanhydride (97%, Aldrich) (recrystallized from acetic acid anhydride), 4,4′-hexafluoroisopropylidenediphthalic anhydride (99%, Aldrich) (recrystallized from acetic acid anhydride), 3,3′,4,4′-biphenyltetracarboxylic dianhydride (99%, Ak Scientific) (recrystallized from acetic acid anhydride), isoquinoline (97%, Aldrich), 1-methyl-2-pyrrolidinone (99.5%, anhydrous, Aldrich), *m*-cresol (Riedel de-Haen) (purified by vacuum distillation), dimethyl sulfoxide (99.9%, anhydrous, Aldrich), ethanol (99.5% Aldrich), chloroform (98% Merck), tetrahydrofuran (99.9%, anhydrous, inhibitor-free, Aldrich), and *N*,*N*-dimethylformamide (99.8%, anhydrous Aldrich).

Synthesis. Equimolar amounts of the monomers (typically ∼1 g of BINAM or FDA) were dissolved in 10 mL of freshly distilled *m*-cresol under an argon atmosphere. Then 2 mL of dry toluene was added and 0.1 mL of isoquinoline as a catalyst. Then the solution was stirred at 80 °C for 1 h and then at 200 °C for 5 h under an inert gas atmosphere. A Dean−Stark trap was used to separate the water which was produced during the reaction. After cooling to room temperature, the polymer solution was slowly dripped into ethanol. The crude product was separated as a precipitate, dried, and reprecipitated from chloroform into ethanol three times. Finally, the products were dried under high vacuum. The polymer FDA-PMDA could not be dissolved in chloroform and was therefore reprecipitated from NMP into ethanol.

Methods. WAXS measurements were performed with a D8 Advance machine from Bruker Instruments. The Cu Kα radiation was used (λ = 0.154 nm). Patterns were collected in reflection geometry. Samples were measured as fine powders or films on a silicon sample holder.

SAXS on solid samples was measured with the Nonius Rotating Anode Instrument (4 kW, Cu Kα) with pinhole collimation and MARCCD detector (pixel size 79) at room temperature and a distance of 33.8 cm between detector and sample, covering a range of the scattering vector $q = 4\pi\lambda^{-1}\sin(\theta)$ from 0.65 to 8.9 nm^{-1} (2θ: scattering angle, λ = 0.154 nm). The observed scattering patterns were corrected for empty-beam scattering. The 2D diffraction patterns were transformed into a 1D radial average of the scattering intensity using the Fit2D software. Nitrogen (at 77 K), argon (at 77 K), and carbon dioxide (at 273 K) sorption measurements were performed using an Autosorb-1MP machine by Quantachrome instruments. Samples were outgassed at 150 °C under high vacuum ($<10^{-7}$ bar) for ∼16 h prior to measurement. Data analysis was performed using the AS1Win software from Quantachrome instruments.

Hydrogen adsorption isotherms at 77 K up to 1 bar were measured using an Autosorb 1C apparatus (Quantachrome) using 99.999% pure gas. Prior to the measurements, the samples were evacuated at high vacuum and 120 °C for 24 h.

DSC measurements were performed on a Netzsch DSC Phoenix in an inert nitrogen atmosphere at a heating rate of 10 K min^{-1}. TGA on the decomposition temperature was carried out on a Netzsch TG 209 F1 at 20 K min^{-1} under a nitrogen atmosphere. EA was measured with a machine Micro from Vario.

FT-IR spectra were collected with a Varian1000 FT-IR (scimitar series) spectrometer, equipped with an attenuated total reflection (ATR) setup.

GPC in 0.5 wt % LiBr in NMP as the eluent was performed with a system containing PSS GRAM 100 and 1000 Å columns under simultaneous UV and RI detection. 100 μL was injected and separated at 70 °C and a flow of 0.8 mL min^{-1}. GPC in DMSO as the eluent was performed with a system containing two PSS GRAL LIN columns. It provides simultaneous UV and RI detection. 100 μL was injected and separated at 70 °C and a flow of 1.0 mL min^{-1}. Samples were filtered through 0.45 μm syringe filters prior to use.

Ellipsometry measurements were performed on a thin film of BINAM−PMDA on a silicon wafer spin-cast from 0.1 wt % solution of BINAM−PMDA in chloroform (60 s, 6000 rpm). Ellipsometry measurements were performed using an Optrel Multiskop ellipsometer. The sample was positioned in a glass chamber which allowed the control of the atmosphere. Data processing was performed using the Multic 832 software.

RESULTS AND DISCUSSION

Polymer Synthesis and General Polymer Properties. The poly(imide)s were synthesized in a one-step synthesis using isoquinoline as catalyst. *m*-Cresol was chosen as solvent. Toluene was used as a cosolvent to allow azeotropic water removal. A Dean−Stark trap was used for effective water separation. BINAM and FDA were reacted with pyromellitic dianhydride (PMDA), 4,4′-oxidiphthalic anhydride (ODPA), 4,4′-(hexafluoroisopropylidene)diphthalic anhydride (6FDA), and 3,3′,4,4′-biphenyltetracarboxylic dianhydride (BPDA). These comonomers introduce different properties into the polymer chain. PMDA can be regarded as a short and stiff linker. BPDA is a longer linker and probably less stiff than PMDA due to the single bond of the biphenyle. 6FDA is also a long linker and introduces an additional kink into the polymer chain. It can also be regarded as a rather stiff monomer as the CF_3 groups hinder rotations. Contrary, ODPA is the most flexible monomer due to its ether bond. Figure 1 summarizes the structures of the monomers. The polymer nomenclature is defined by the used monomers; i.e., BINAM−PMDA describes a polyimide obtained by reaction of BINAM with PMDA.

The products were analyzed by infrared spectroscopy (IR) to validate the chemical structure (Figures S1 and S2). Nuclear magnetic resonance (NMR) measurements were also performed but could not be used as a precise tool for the polymer analysis as coupling of the aromatic rings in the chain led to many peaks which could not be exactly distinguished. However, no signal originating from amide groups (NH) or carboxylic acids (COOH) could be detected. On the basis of the spectroscopic investigations, a successful imidization is proven. Molecular weights and molecular weight distributions were determined by gel permeation chromatography (GPC) in DMSO against PMMA standards (see Table S1). The data obtained by GPC have to be regarded as relative, only, since the chemical and structural composition of the used standard differs significantly from the analyte but gives nevertheless an estimate of the molecular weights.

The solubility of the polymers was tested in a variety of solvents. As expected, polar solvents such as *m*-cresol or NMP were good solvents for all polymers, while ethanol, methanol, and acetone are nonsolvents. Chloroform and bromoform were also good solvents except for the partial crystalline FDA−PMDA. THF could solubilize only a few of the poly(imide)s. The molecular weight characteristics and the solubility of the polymers are summarized in Table 1.

All polymers have polydispersities between 1.5 and 2.2. Polydispersities smaller than 2 can be explained by fractionation effects during reprecipitation. Generally, the molecular weights of the FDA poly(imide)s were much higher (1 order of magnitude) than those of the BINAM poly(imide)s. This became also obvious when polymer films were cast. FDA-based poly(imide)s gave mechanically stable films, while no free-standing films could be formed from BINAM poly(imide)s. The obtained low molecular weights of the BINAM poly(imide)s might be explained by geometric arguments. From simple molecular modeling, it is obvious that the condensing polymer chains form rather compact coils (Figure S4). As the polymer chains are stiff, it can be imagined that the accessibility of the end groups which

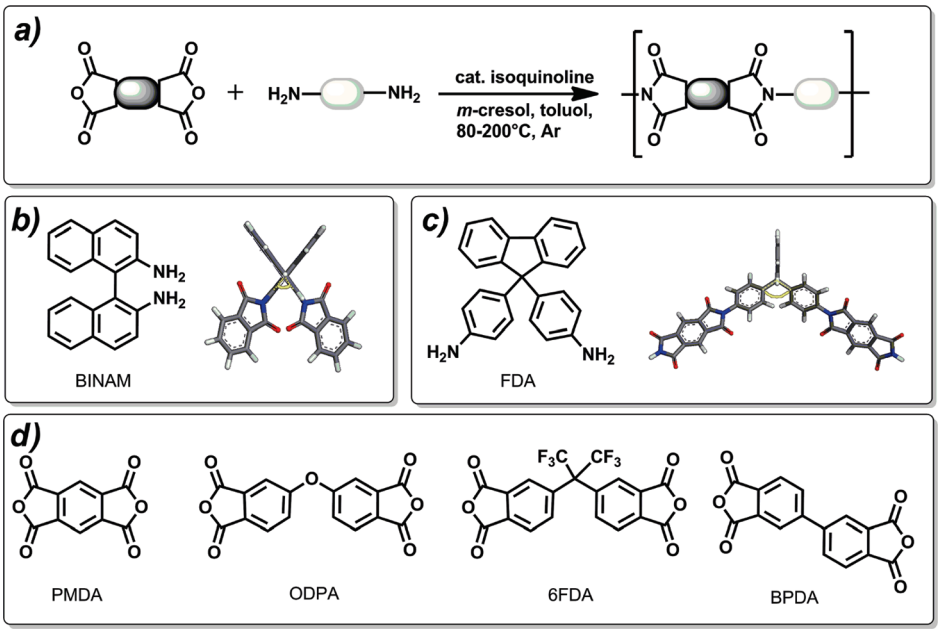

Figure 1. (a) General synthesis of poly(imide)s. (b) Chemical structure of BINAM and a geometry-optimized 3D model of its phthalimide. (c) Chemical structure of FDA and a geometry-optimized 3D model of its phthalimide. (d) Chemical structures of the used dianhydride monomers.

Table 1. Molecular Weights, Polydispersity, and Room Temperature Solubility of the Poly(imide)s[a]

sample	M_w (g/mol)	PDI	THF	$CHCl_3$	NMP	DMSO	DMF	*m*-cresol
BINAM−PMDA	11 060	1.8	×	√	√	√	√	√
BINAM−ODPA	9 300	1.6	√	√	√	√	√	√
BINAM−6FDA	10 500	1.6	√	√	√	√	√	√
BINAM−BPDA	10 300	1.4	×	√	√	√	√	√
FDA−PMDA			×	×	√[b]	×	×	√[b]
FDA−ODPA	82 400	1.9	×	√	√	√	√	√
FDA−6FDA	78 500	2.2	√	√	√	√	√	√
FDA−BPDA			×	√	√	×	×	√

[a] M_w and PDI determined by GPC using DMSO as eluent. [b] Soluble at 100 °C.

have to react in order to form higher molecular weight chains is limited by geometric exclusion. The observation of only moderate molecular weights for binaphthalene-based polycondensates was reported already previously[42,43] and seems to be an intrinsic problem of binaphthalene monomers. FDA has a larger kink angle, and modeling reveals less compact polymer chains. Consequently, end groups might be better accessible which leads to higher molecular weights. The synthesis of BINAM−PMDA gave cyclic byproducts, as reported already earlier.[38] Reprecipitation was used to remove them due to their poor solubility. For the other polyimides, there was no clear indication of cyclic byproducts, although their presence cannot be excluded.

Thermal analysis of the polymers revealed high-temperature stability (decomposition onset under nitrogen atmosphere ≥500 °C). Glass transitions (~380 °C) could only be measured for ODPA and 6FDA containing polyimides.

Wide-angle X-ray scattering (WAXS) could prove that all polyimides except FDA−PMDA were amorphous. Typically, two halos at scattering angles 2θ around 10−15° and 20−25° were observed. For FDA−PMDA a number of peaks could be identified together with a broad amorphous halo, which indicates that FDA−PMDA is partially crystalline. This feature is also reflected in the poor solubility of FDA−PMDA. Details of the WAXS patterns will be discussed later.

Gas Sorption. First, we will discuss the gas sorption properties of materials that were precipitated from solution. The sorption behavior of solution cast films will be discussed later. We used various gases (N_2, Ar, H_2, CO_2) to achieve a more complete picture of the materials porosity. N_2, Ar, and H_2 adsorption/desorption isotherms were collected at 77 K. CO_2 sorption was measured at 273 K.

N_2 and Ar sorption at 77 K can give information about a broader size range of micro- and mesopores. However, the measurements tend to be very slow, and it is known that nitrogen sorption on ultramicroporous samples (pores <0.8 nm) can underestimate the microporosity and is sometimes affected by kinetic effects.[44,45] Hydrogen sorption at 77 K and CO_2 sorption at 273 K can give valuable information on micropores, also on those that cannot be probed by classic N_2 sorption.[45] Both methods have already been applied to the analysis of microporous polymers,[38,41,46−48] but more knowledge is needed to estimate their feasibility and also their limitations.

Figure 2 shows the N_2 and Ar sorption isotherms of precipitated poly(imide)s. For the BINAM-based polymers, only PMDA and

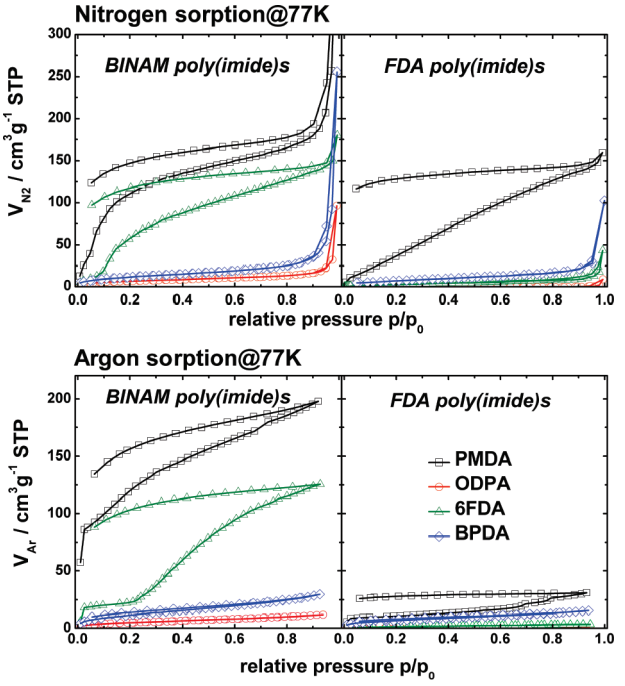

Figure 2. Nitrogen (upper part) and argon (lower part) adsorption/desorption isotherms of BINAM poly(imide)s (left-hand side) and FDA poly(imides) (right-hand side). The isotherms were collected at 77.3 K.

6FDA poly(imide)s showed a significant uptake of nitrogen and argon. The isotherms did not close upon desorption in the measured pressure range, thus yielding a large hysteresis down to low relative pressures. For BINAM−6FDA it was observed that the uptake of nitrogen and argon due to the microporosity was shifted to higher relative pressures (p/p_0 = 0.1 for N_2, p/p_0 = 0.2 for Ar), which might be indicative for some kind of gating effect. For BINAM−PMDA the influence of the measurement protocol was checked by applying different adsorption conditions. Interestingly, the isotherms differed significantly in the adsorption branch, but the same overall uptake and desorption pattern was found, irrespective of the different adsorption protocol (see Figure S5). It should be noted, furthermore, that we reported in a former communication that BINAM−PMDA is not capable of adsorbing significant amounts of nitrogen.[38] While the polyimide reported formerly was prepared via the polyamic acid route, the BINAM−PMDA currently under investigation was prepared by the optimized solution polycondensation in *m*-cresol. It is probably due to subtle differences in the degree of imidization that different gas sorption behavior can be detected.

Of all of the FDA poly(imide)s, only FDA−PMDA showed a significant nitrogen uptake. The adsorption pattern is however a rather uncommon one, as the adsorbed volume increases almost linearly with relative pressure. This might be related to kinetic restrictions; i.e., the diffusion of nitrogen into the inner pores is slowed down. Upon desorption, again a large hysteresis down to low relative pressures was observed. Finally, no uptake of Ar which could be attributed to the presence of micropores could be observed for FDA poly(imide)s. Because of the observed uncommon sorption isotherms, no further analysis of the N_2 and Ar sorption data was performed.

The sorption of hydrogen at 77 K can be regarded as an additional analytical tool for microporous polymers.[9] For hypercross-linked poly(aniline) and PIM-type poly(amide) it is known

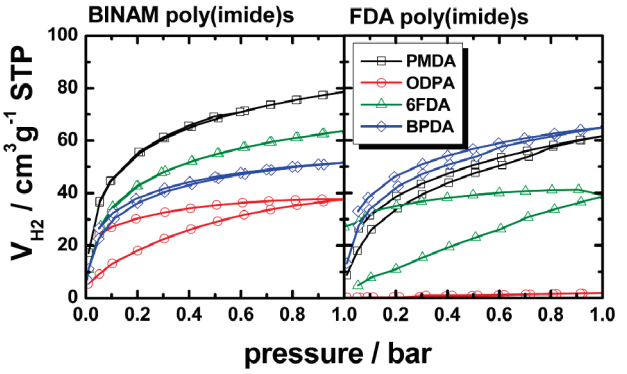

Figure 3. Hydrogen adsorption/desorption isotherms of BINAM poly(imide)s (left-hand side) and FDA poly(imides) (right-hand side). The isotherms were collected at 77.3 K.

that hydrogen can also enter pores which are inaccessible for nitrogen,[8,46] which is probably due to its much smaller kinetic diameter (2.9 Å for H_2 and 3.6 Å for N_2). Therefore, we were interested in the hydrogen adsorption properties of the poly(imide)s under investigation. Figure 3 shows the hydrogen adsorption and desorption isotherms of the poly(imide)s. Numerical values derived from the adsorption isotherms are summarized in Table 2.

All BINAM poly(imide)s showed significant uptake of hydrogen. The order of uptake was PMDA > 6FDA > BPDA > ODPA. More interestingly, BINAM−PMDA and BINAM−6FDA did not feature a hysteresis upon desorption, while a hysteresis was observed for BINAM−BPDA and BINAM−ODPA. Having in mind that BINAM−PMDA and BINAM−6FDA were also capable of adsorbing the larger nitrogen molecules, we speculate that the hysteresis might be due to kinetic trapping of hydrogen in very narrow pores upon desorption. In the case of FDA poly(imide)s, comparable hydrogen uptake was found for PMDA and BPDA. FDA−6FDA showed lower hydrogen uptake, comparable to BINAM−ODPA. Finally, no hydrogen uptake was found for FDA−ODPA. For all FDA poly(imide)s that showed hydrogen uptake, a hysteresis was observed, which relates probably back to the same reason as described above. From the hydrogen sorption isotherms, one can already draw a more general picture of the impact of the polymer architecture on the observable porosity. Flexible comonomers as ODPA lead to polymers of only small or no accessible porosity, which marks the limit of intrinsic microporosity. Short and stiff linkers, such as PMDA, serve well as building blocks for intrinsic microporosity. Larger, stiff comonomers (6FDA and BPDA) lead to lower porosity compared to the shorter connecting monomers. A probable reason for this might be intercalation of kinked polymer chains, which would close pores. Regarding the kink angle, it can be stated that a larger kink angle (∼109° for FDA compared to ∼77° for BINAM or ∼90° for spiro compounds) leads to more elongated chains rather than highly contorted ones, which again favors close packing and/or intercalation.

The adsorption isotherms were fitted by the Langmuir model as well as by a dual-mode sorption model in order to obtain information on the specific surface areas of the materials. The Langmuir model is used frequently to determine specific surface areas of microporous polymers from hydrogen sorption isotherms.[24,38,46] However, the model has some drawbacks, as microporous polymers usually do not feature a homogeneous surface (i.e., the sorption places are energetically different). Furthermore, only little is known

Table 2. Specific Surface Areas of the Poly(imide)s Determined by Various Models from the H_2 and CO_2 Adsorption Isotherms

entry	$S_{H_2,L}$ ($m^2\ g^{-1}$)	$S_{H_2,DM}$ ($m^2\ g^{-1}$)	H_2 uptake (wt %)	$S_{CO_2,L}$ ($m^2\ g^{-1}$)	$S_{CO_2,DM}$ ($m^2\ g^{-1}$)	$S_{CO_2,DFT}$ ($m^2\ g^{-1}$)	$S_{CO_2,GCMC}$ ($m^2\ g^{-1}$)
BINAM−PMDA	225	167	0.7	274	152	380	370
BINAM−ODPA[b]	135	69	0.34	133	72	178	177
BINAM−6FDA	188	141	0.58	170	90	220	210
BINAM−BPDA[a]	149	111	0.46	192	134	255	245
FDA−PMDA[b]	198	103	0.56	314	155	400	390
FDA−ODPA[a]			0.016	192	88	230	245
FDA−6FDA[b]	301	22	0.36	221	109	290	270
FDA−BPDA[b]	189	125	0.58	230	129	330	310

[a] Significant hysteresis upon CO_2 desorption. [b] Significant hysteresis upon H_2 desorption.

about the state of hydrogen confined within very small pores, and there are still controversies about this issue.[45,49] Third, it was shown that diffusion of hydrogen into the inner part of small pore systems can occur through a hopping mechanism, which also affects the observed isotherms.[50] We used the dual-mode model as developed for gas uptake in polymeric membranes to account for these effects. The dual-mode model assumes that gas uptake in polymeric membranes occurs by two mechanisms.[51] One is the filling of void spaces according to the Langmuir law, and the other one describes the dissolution of gas in the polymer matrix which follows Henry's law. Accordingly, the total gas uptake is described as the sum of both contributions: $V_{total} = V_{Langmuir} + V_{Henry}$.

Usually, the dissolution of gases in the polymer matrix is observed at high pressures, i.e., higher than atmospheric pressure. Nevertheless, the introduction of the linear term might compensate the above-mentioned drawbacks of a pure Langmuir approach. It can be imagined that the occupation of very narrow micropores (which might even need small reorientations of the polymer chains) is phenomenologically comparable to the dissolution of gas in the matrix. The use of the dual-mode approach allows also the extraction of the specific surface area of the polymers based on its Langmuir term, in analogy to a pure Langmuir model. The results are summarized in Table 2 (please see the Supporting Information for full fit parameters and plots). Generally, the dual-mode approach yields better fits of the hydrogen adsorption data ($R^2 > 0.99$) than the Langmuir model ($0.97 > R^2 > 0.99$). The derived specific surface area values will be discussed after the introduction of the carbon dioxide sorption results.

Carbon dioxide sorption at 273 K was measured in order to obtain a more complete picture of the microporosity of the materials microporosity. Figure 4a,c depicts the CO_2 adsorption/desorption isotherms of the precipitated samples. The isotherms of the cast samples (Figure 4b,d) will be discussed later.

The highest carbon dioxide uptake was found for PMDA polyimides, and the lowest uptake was found for ODPA polyimides. These results are in good agreement with the results from nitrogen, argon, and hydrogen sorption measurements. Generally, we observed much less hysteretic adsorption compared to the hydrogen sorption experiments. Only BINAM−BPDA and FDA−ODPA showed a significant hysteresis upon desorption. Interestingly, FDA−ODPA took up carbon dioxide while it did not show adsorption activity for hydrogen. Hydrogen has a nominally smaller kinetic diameter (d_{H_2} = 2.89 Å) than carbon dioxide (d_{CO_2} = 3.3 Å); hence, this result indicates that solubility plays a crucial role next to the overall porosity in carbon dioxide sorption.[52,53] Furthermore, the dynamics of the polymer chains are different at 77 and 273 K. This might also influence the sorption properties and will be discussed in detail later.

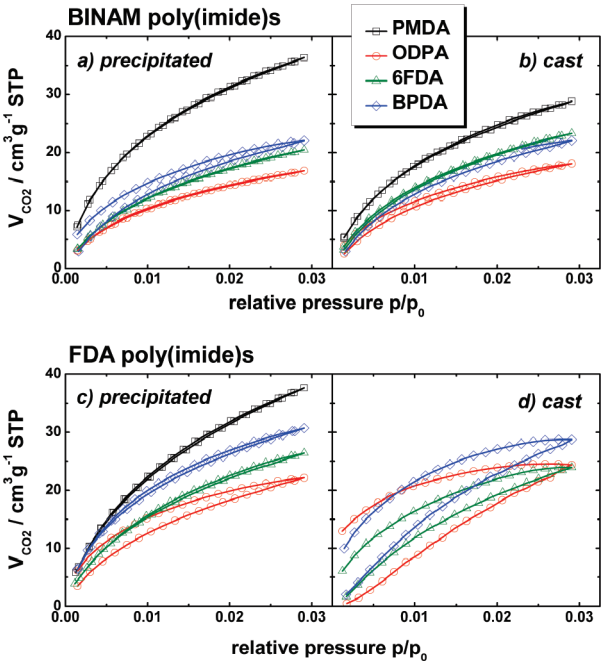

Figure 4. Carbon dioxide adsorption/desorption isotherms of precipitated (a) or cast (b) BINAM poly(imide)s and precipitated (c) or cast (d) FDA poly(imides). The isotherms were collected at 273.15 K.

The CO_2 adsorption data were also analyzed by applying the Langmuir and the dual-mode sorption model. As poly(imide)s are known to have a good solubility for CO_2,[54,52,53] the dual-mode sorption model was expected to be more reliable. The data could however be fitted very well by both approaches with $R^2 > 0.994$ for the Langmuir model and $R^2 > 0.9998$ for the dual-mode model. Recently, NLDFT and GCMC kernels were developed for the analysis of CO_2 sorption isotherms of carbonaceous microporous materials.[55,56] These models take condensation within micropores into account and allow the extraction of a pore size distribution (PSD) as well as the determination of the specific surface area of the adsorbent. Table 2 summarizes the specific surface areas of the poly(imide)s as determined by the various methods.

Fitting of the hydrogen and carbon dioxide adsorption isotherms by the Langmuir equation gives values for the specific surface areas of up to 300 $m^2\ g^{-1}$. Specific surface areas obtained by the NLDFT and GCMC models give the highest values (up to 400 $m^2\ g^{-1}$) but are generally in agreement with the Langmuir surface areas. As all of the applied models have several advantages

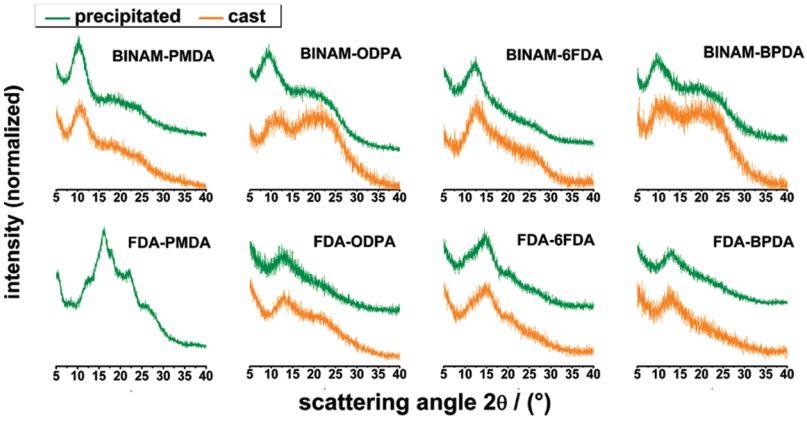

Figure 5. WAXS data for precipitated and cast BINAM and FDA poly(imide)s; precipitated from chloroform into ethanol (upper patterns) and solvent cast from chloroform (lower patterns); for better comparability patterns were normalized for maximum halo intensity and vertically offset.

and drawbacks, we would not highlight one of the methods as the method of choice.

Pore size distributions were determined from the CO_2 sorption isotherms by models derived from NLDFT and GCMC (Figures S5 and S6).[55] Both models yield comparable pore size distributions. The models suggest that the main fraction of pores has radii between 2 and 4 Å. These radii are well comparable to the typical FVE sizes of other high-free volume polymers.[57] From the obtained PSDs, it is however not possible to draw any relation between the nature of the comonomer and the observable pore sizes.

Finally, the comparison of the difference in the sorption behavior of the BINAM and FDA poly(imide)s with regard to nitrogen or argon and carbon dioxide or hydrogen leads to the conclusion that nitrogen molecules and argon atoms are too big and/or too slow to diffuse easily into very small pores. In contrast, hydrogen and carbon dioxide have a smaller kinetic diameter and a higher kinetic energy, which allows them to enter these pores. Generally, it can be stated that nitrogen and argon are suitable to characterize pores which are bigger than 10 Å, while hydrogen and carbon dioxide sorption are more suitable for ultramicropores. The determined pore sizes are generally well comparable with pore sizes of other high free volume polymers, which are most often also ultramicroporous.[57]

Influence of Processing. We showed already previously that processing can have an influence on the observable porosity of microporous polymers.[37,38] Hence, the question arose whether BINAM and FDA polymers would behave similarly. Samples were either precipitated into ethanol from chloroform solution or cast from chloroform. For FDA−PMDA no films were cast due to its poor solubility in chloroform.

To investigate microstructural differences, we measured the wide-angle X-ray scattering (WAXS) patterns of the samples. Small-angle X-ray scattering (SAXS) was also employed to cover a wide range of scattering vector. SAXS patterns could however only give limited information as Porod behavior was observed in the case of the precipitated samples. This is due to the formation of particles upon precipitation and overlays the region of interest. Therefore, the SAXS patterns of the cast poly(imide) samples could not be compared with the patterns of the precipitated samples.

WAXS measurements have been performed on both precipitated and cast samples. Generally, WAXS is a fast method and can be applied to study porous materials. However, the interpretation of amorphous halos of polymers is still discussed. While halos in poly(imide)s are for instance discussed to arise from interchain or intersegmental separation,[58] there are also reports which discuss intramolecular electron density fluctuations with well-defined separation distances as the origin of observed halos.[59,60] Microporous polymers show often multiple halos. Typically, there is a halo at lower scattering angles and one at higher scattering angles. The halo at higher angles is accredited to the chain-to-chain distance of space efficient packed chains and the halo at lower scattering angles to more loosely packed polymer chains, i.e., to segments keeping their conformation with the micropores in between.[34,37,38] WAXS patterns of the poly(imides) are given in Figure 4.

In the case of all BINAM polymers, two halos were found: the first one at scattering angles around 9°−12.5° and the second one at 20°−25° (Figure 4). FDA−PMDA was found to be semicrystalline, while the other FDA polymers showed one amorphous halo around 13°−15° (Figure 5). A second halo between 20° and 25° seems to be present but cannot be identified clearly. There is a trend in the position of the first halo at lower angles when comparing BINAM and FDA polymers. The halo is found at lower angles for BINAM polyimides, which would correspond to a larger separation distance between the polymer chains. On the other hand, when comparing the gas sorption properties of e.g. BINAM−BPDA and FDA−BPDA, it is found that FDA−BPDA has a higher H_2 and CO_2 uptake. Furthermore, evaluation of the PSDs from CO_2 sorption did not give any evidence of significant differences between BINAM and FDA poly(imide)s (see Figures S5 and S6). Hence, the position of the first halo cannot be solely ascribed to the interchain separation but is most probably also influenced by the molecular structure, i.e., intramolecular distances.

Upon solution casting, the intensity of the halo at small scattering angles decreases relative to the intensity of the second halo in most cases. This effect is most prominent in BINAM−ODPA and BINAM−BPDA, but it is also observed in other cases. For instance, the second halo in the WAXS pattern of FDA−ODPA just becomes visible for the solvent-cast sample. However, only little effect is observed for BINAM−6FDA and FDA−6FDA. It was reported that the WAXS patterns of 6FDA containing poly(imide)s can be dominated by the presence of the fluorine atoms.[60] Hence, no clear interpretation is possible for the 6FDA containing poly(imide)s. Even though there is still discussion about the specific meanings of the halos, it can be safely stated that the microstructure of the system can be different when cast and when precipitated.

We also determined the respective *d*-spacings, which are frequently used as a measure of the density of chain packing (see Table S3). While the *d*-spacings do often show a good correlation

to other parameters (e.g., gas permeability), we did not observe such a correlation toward the porosity. For instance, FDA−ODPA and FDA−BPDA have the same *d*-spacing (~6.9 Å); however, it is only FDA−BPDA that shows a significant H_2 uptake. FDA−6FDA does even feature a smaller *d*-spacing (6.0 Å) compared to FDA−BPDA, but it does adsorb comparable amounts of CO_2. These examples show that the *d*-spacing alone cannot be a measure of porosity and is not discussed in more detail in this paper.

Hydrogen and carbon dioxide sorption measurements were furthermore performed to characterize eventual differences in the sorption behavior depending on the processing of the sample. The hydrogen uptake of the cast polymer samples is significantly lower than for the comparable precipitated polymers and almost negligible (see Figure S7). Because of the lower outer surface of the cast samples, the diffusion of hydrogen, supposedly due to intersite hopping, is suggested to be very slow.[50] However, the difference in hydrogen sorption isotherms of cast and precipitated samples is so significant that this effect is presumably not the major cause.[61] Instead, it is suggested that a change of the polymer microstructure upon processing influences the hydrogen sorption ability of the cast polymers. This is in accordance with the observed WAXS patterns.

Most interestingly, the CO_2 uptake was however significant also for cast samples (see Figure 4b,d). Only for BINAM−PMDA a smaller total uptake (~20% smaller) was observed, while all other poly(imide)s showed generally comparable uptakes irrespective of their processing. In the case of FDA poly(imide)s a pronounced hysteresis was observed upon desorption. We attribute this hysteresis mostly to diffusion effects. These might originate from the higher molecular weights of the FDA polymers which lead to higher entanglements.

There are a variety of possible explanations for the observed high CO_2 uptake. First, it is recognized that some poly(imide) membranes are sensitive to CO_2 plasticization and that some of them adsorb CO_2 even at low pressures.[54,62] Therefore, the interactions of the highly polar imide functionalities and carbon dioxide with its considerable quadrupolar moment cannot be neglected and might enhance the solubility and entrance of CO_2 in the poly(imide) membranes. Second, we have to keep in mind that the H_2 and CO_2 sorption measurements are undertaken at completely different temperatures, an effect that was not paid attention up to now. Although the poly(imide)s are far below their glass transition temperature, they are not completely immobile; i.e., thermal motion is still present. From dynamic mechanical analysis, it is known that the γ-relaxation of aromatic poly(imide)s is found between 123 and 173 K. The onset of the β-relaxation is for certain FDA poly(imide)s also below 273 K.[63] In other words, the poly(imide)s are deeply frozen at 77 K but can most probably undergo some relaxations at 273 K.

It might be stated that the Langmuir sites which are filled by gas can be differentiated by "static" Langmuir sites (low *T*) and "dynamic" Langmuir sites (high *T*). Static holes can be filled by gas molecules if they are open to the outside and large enough to allow gas molecules to enter. Contrary, at higher temperatures, the holes might adopt in size or shape to fit the incoming molecules and can be termed dynamic Langmuir sites. In order to further analyze this effect, we measured the N_2 uptake of selected samples at 273 K and found significant gas uptake which is an indicative of microporosity (see Figure S8 and Table S4). It is possible to determine the apparent CO_2 over N_2 selectivity at 273 K. Values varying between 20 and 30 were observed for BINAM−ODPA, BINAM−BPDA, and FDA−BPDA. Such small values are typical for the absence of molecular sieving effects;[64] i.e., the N_2 molecules can indeed enter the micropore system at 273 K even if they cannot do so at 77 K. For FDA−ODPA a higher selectivity (~50) was found, pointing to the transition toward size restricted access. As FDA−ODPA is the least porous material of all analyzed materials, this finding is in line with the low-temperature H_2 sorption.

Scheme 1. Overview on the Observed Differences in Gas Uptake upon Different Processing (Upper Part) and Sketch of the Underlying Temperature Dependent Microstructure

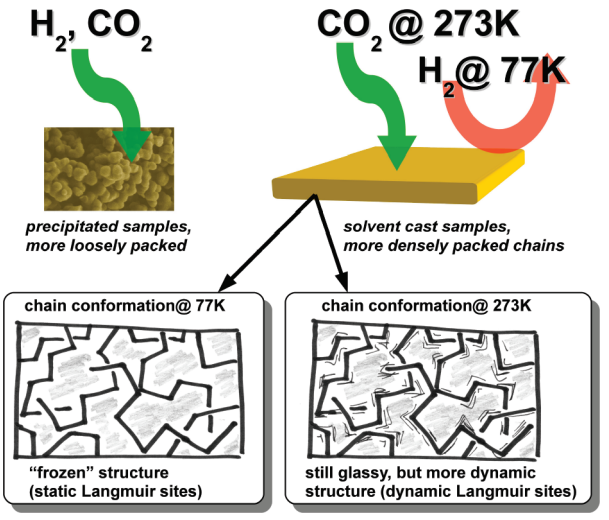

Positive interactions (solubility effects) between the adsorbent and adsorbate might even facilitate the gas uptake process. This raises however the question on the applicability of NLDFT or GCMC models developed for CO_2 sorption analysis. In the present study, we did not observe any significant difference in the PSD obtained from the different poly(imide)s, which most probably does not reflect reality and is in contrast to results obtained from CO_2 sorption on other polymers.[48] As only limited experimental data on CO_2 sorption in microporous polymers is available up to now, we do however not want to draw final conclusions on this issue within the present study.

Finally, processing can influence the accessibility of the sorption sites. Upon precipitation, we find a more open, loosely packed morphology while solvent casting leads to a more dense morphology which is presumably thermodynamically more stable. Scheme 1 summarizes these findings.

CONCLUSIONS

It was shown that ultramicroporous poly(imide)s can be prepared by using BINAM and FDA monomers. However, molecular weights of BINAM-based poly(imide)s were 1 order of magnitude lower than that of FDA poly(imide)s. This might be ascribed to the steric constraints of the monomer and is consistent with other reports on binaphthalene-based polymers. The resulting poly(imide)s showed, contrary to other fully aromatic poly(imide)s, good solubility in a broad variety of organic solvents, which can be attributed to their contorted structure which permits space-efficient packing.

This work focused on a detailed investigation of the porosity of soluble microporous polymers. The polyimides were analyzed by gas sorption using nitrogen, argon, hydrogen, and carbon dioxide

and wide-angle X-ray scattering. It could be shown that nitrogen and argon sorption measurements are not suitable to reliable detect pores in the size range of interest (3−10 Å). Hydrogen and carbon dioxide sorption are tools which can detect pores in this size range. However, both of these methods must be regarded with care as well. Hydrogen sorption isotherms could not be well fitted by a simple Langmuir approach, indicating that condensation or multilayer formation might be active. Carbon dioxide sorption could also be used successfully. However, interactions between the quadrupolar carbon dioxide and the poly(imide)s must be taken into account as well as the higher mobility of the polymer segments at the measurement temperature.

When comparing the porosity of BINAM or FDA polymers which are built up with the different comonomers, a trend connecting porosity and the comonomer unit can be seen. The highest free volume was found for PMDA poly(imide)s, followed by 6FDA, BPDA, and ODPA. PMDA is a stiff and short linker. While BPDA and 6FDA are also stiff, their length might allow intercalation of the polymer chains. The kink in 6FDA could lead a better accessibility of pores than BPDA in the case of BINAM as the monomer; in the case of FDA, it is the other way round. Since ODPA is flexible, polymer chains can pack more closely, setting a limit to intrinsic microporosity. No order of porosity was found for BINAM and FDA polymers when reacted with the same comonomers. Whether the respective BINAM or FDA poly(imide) contains more micropores is determined by the overall structure of the polymer.

Processing has a huge influence on the observable porosity. BINAM and FDA polymers showed different properties after being solvent cast or precipitated. WAXS could give qualitative information about the microstructure of the poly(imide)s. Because of a probable overlap of various scattering contributions, it is however not possible to draw conclusions from WAXS patterns alone. BINAM and FDA polymers took up comparable amounts of carbon dioxide irrespective of their processing but did not adsorb hydrogen or nitrogen when being solvent cast. This was partially explained by the higher mobility (dynamic sorption sites) of the polymers at 273 K (the typical CO_2 sorption measurement temperature) compared to the frozen structure at 77 K (the typical N_2/H_2 sorption measurement temperature). This effect needs clarification and more experiments needs to be done for understanding.

In summary, the present work tried to shed light on the borderline between nonporous and intrinsically microporous poly(imide)s. It was shown that carbon dioxide and hydrogen sorption are very helpful tools when it comes down to ultramicropores. Future work will also concentrate on the gas permeation properties of some of the here presented polymers as well as on the polymer physics under changing atmospheres. Preliminary investigations of the response of a thin film of BINAM−PMDA to changing gas atmospheres by ellipsometry indicated that the poly(imide)s undergo some microstructure changes upon gas adsorption (see Figure S9). The possibility to use this optical response to outer stimuli in sensor application will be also investigated.

■ ASSOCIATED CONTENT

Supporting Information. Spectroscopic data, gas adsorption analysis, and ellipsometry data. This material is available free of charge via the Internet at http://pubs.acs.org.

■ AUTHOR INFORMATION

Corresponding Author

*Fax +49-331-5679502, phone +49-331-5679569, e-mail jens.weber@mpikg.mpg.de.

■ ACKNOWLEDGMENT

We thank Marlies Gräwert for GPC measurements, Irina Shekova for thermal analysis, and Dr. Antonio Stocco for support with the ellipsometry experiments. Prof. Markus Antonietti is acknowledged for helpful discussions. Financial support from the ENERCHEM projects of the Max Planck Society is gratefully acknowledged.

■ REFERENCES

(1) Thomas, A.; Kuhn, P.; Weber, J.; Titirici, M.; Antonietti, M. *Macromol. Rapid Commun.* **2009**, *30*, 221–236.
(2) McKeown, N. B.; Budd, P. M. *Macromolecules* **2010**, *43*, 5163–5176.
(3) Cooper, A. I. *Adv. Mater.* **2009**, *21*, 1291–1295.
(4) Ghanem, B. S.; Kadhum, J.; McKeown, N. B.; Harris, K.; Pan, Z.; Budd, P.; Butler, A.; Selbie, J.; Book, D.; Walton, A. *Chem. Commun.* **2007**, 67–69.
(5) McKeown, N. B.; Hanif, S.; Msayib, K.; Tattershall, C. E.; Budd, P. M. *Chem. Commun.* **2002**, 2782–2783.
(6) McKeown, N. B.; Makhseed, S.; Budd, P. M. *Chem. Commun.* **2002**, 2780–2781.
(7) Farha, O. K.; Spokoyny, A. M.; Hauser, B. G.; Bae, Y.; Brown, S. E.; Snurr, R. Q.; Mirkin, C. A.; Hupp, J. T. *Chem. Mater.* **2009**, *21*, 3033–3035.
(8) Weber, J.; Antonietti, M.; Thomas, A. *Macromolecules* **2008**, *41*, 2880–2885.
(9) Germain, J.; Frechet, J. M. J.; Svec, F. *J. Mater. Chem.* **2007**, *17*, 4989–4997.
(10) Schmidt, J.; Weber, J.; Epping, J.; Antonietti, M.; Thomas, A. *Adv. Mater.* **2009**, *21*, 702–705.
(11) Weber, J.; Thomas, A. *J. Am. Chem. Soc.* **2008**, *130*, 6334–6335.
(12) Jiang, J. X.; Su, F.; Trewin, A.; Wood, C. D.; Niu, H.; Jones, J.; Khimyak, Y. Z.; Cooper, A. I. *J. Am. Chem. Soc.* **2008**, *130*, 7710–7720.
(13) Chen, L.; Honsho, Y.; Seki, S.; Jiang, D. *J. Am. Chem. Soc.* **2010**, *132*, 6742–6748.
(14) Dawson, R.; Laybourn, A.; Clowes, R.; Khimyak, Y. Z.; Adams, D. J.; Cooper, A. I. *Macromolecules* **2009**, *42*, 8809–8816.
(15) Rose, M.; Bohlmann, W.; Sabo, M.; Kaskel, S. *Chem. Commun.* **2008**, 2462–2464.
(16) Stöckel, E.; Wu, X.; Trewin, A.; Wood, C. D.; Clowes, R.; Campbell, N. L.; Jones, J.; Khimyak, Y. Z.; Adams, D.; Cooper, A. I. *Chem. Commun.* **2009**, 212–214.
(17) Webster, O. W.; Gentry, F. P.; Farlee, R. D.; Smart, B. E. *Makromol. Chem., Macromol. Symp.* **1992**, *54*−*5*, 477–482.
(18) Urban, C.; McCord, E. F.; Webster, O. W.; Abrams, L.; Long, H. W.; Gaede, H.; Tang, P.; Pines, A. *Chem. Mater.* **1995**, *7*, 1325–1332.
(19) Tsyurupa, M. P.; Davankov, V. A. *React. Funct. Polym.* **2006**, *66*, 768–779.
(20) Tsyurupa, M. P.; Davankov, V. A. *React. Funct. Polym.* **2002**, *53*, 193–203.
(21) Ben, T.; Ren, H.; Ma, S.; Cao, D.; Lan, J.; Jing, X.; Wang, W.; Xu, J.; Deng, F.; Simmons, J. M.; Qiu, S.; Zhu, G. *Angew. Chem., Int. Ed.* **2009**, *48*, 9457–9460.
(22) Fritsch, J.; Rose, M.; Wollmann, P.; Böhlmann, W.; Kaskel, S. *Materials* **2010**, *3*, 2447–2462.
(23) Germain, J.; Hradil, J.; Frechet, J. M. J.; Svec, F. *Chem. Mater.* **2006**, *18*, 4430–4435.
(24) Wood, C.; Tan, B.; Trewin, A.; Niu, H.; Bradshaw, D.; Rosseinsky, M.; Khimyak, Y.; Campbell, N.; Kirk, R.; Stöckel, E.; Cooper, A. *Chem. Mater.* **2007**, *19*, 2034–2048.

(25) Cote, A. P.; Benin, A. I.; Ockwig, N. W.; O'Keeffe, M.; Matzger, A. J.; Yaghi, O. M. *Science* **2005**, *310*, 1166–1170.
(26) El-Kaderi, H.; Hunt, J.; Mendoza-Cortes, J.; Cote, A. P.; Taylor, R.; O'Keeffe, M.; Yaghi, O. M. *Science* **2007**, *316*, 268–272.
(27) Uribe-Romo, F. J.; Hunt, J. R.; Furukawa, H.; Klöck, C.; O'Keeffe, M.; Yaghi, O. M. *J. Am. Chem. Soc.* **2009**, *131*, 4570–4571.
(28) Wan, S.; Guo, J.; Kim, J.; Ihee, H.; Jiang, D. *Angew. Chem., Int. Ed.* **2008**, *47*, 8826–8830.
(29) Tilford, R.; Mugavero, S., III; Pellechia, P.; Lavigne, J. *Adv. Mater.* **2008**, *20*, 2741–2746.
(30) Kuhn, P.; Antonietti, M.; Thomas, A. *Angew. Chem., Int. Ed.* **2008**, *47*, 3450–3453.
(31) Budd, P. M.; Ghanem, B. S.; Makhseed, S.; McKeown, N. B.; Msayib, K. J.; Tattershall, C. E. *Chem. Commun.* **2004**, 230–231.
(32) Du, N.; Robertson, G. P.; Song, J.; Pinnau, I.; Guiver, M. D. *Macromolecules* **2009**, *42*, 6038–6043.
(33) Du, N.; Robertson, G. P.; Pinnau, I.; Guiver, M. D. *Macromolecules* **2009**, *42*, 6023–6030.
(34) Du, N.; Robertson, G.; Song, J.; Pinnau, I.; Thomas, S.; Guiver, M. *Macromolecules* **2008**, *41*, 9656–9662.
(35) Staiger, C. L.; Pas, S. J.; Hill, A. J.; Cornelius, C. J. *Chem. Mater.* **2008**, *20*, 2606–2608.
(36) McKeown, N. B.; Budd, P. M. *Chem. Soc. Rev.* **2006**, *35*, 675–683.
(37) Weber, J.; Su, O.; Antonietti, M.; Thomas, A. *Macromol. Rapid Commun.* **2007**, *28*, 1871–1876.
(38) Ritter, N.; Antonietti, M.; Thomas, A.; Senkovska, I.; Kaskel, S.; Weber, J. *Macromolecules* **2009**, *42*, 8017.
(39) Ghanem, B. S.; McKeown, N. B.; Budd, P. M.; Al-Harbi, N. M.; Fritsch, D.; Heinrich, K.; Starannikova, L.; Tokarev, A.; Yampolskii, Y. *Macromolecules* **2009**, *42*, 7881–7888.
(40) Korshak, V. V.; Vinogradova, S. V.; Vygodskii, Y. S. *Polym. Rev.* **1974**, *11*, 45.
(41) Weber, J.; Du, N.; Guiver, M. D. *Macromolecules* **2011**.
(42) Schulz, R. C.; Jung, R. H. *Makromol. Chem.* **1968**, *116*, 190–202.
(43) Du, N.; Robertson, G. P.; Pinnau, I.; Thomas, S.; Guiver, M. D. *Macromol. Rapid Commun.* **2009**, *30*, 584–588.
(44) Lozano-Castelló, D.; Cazorla-Amorós, D.; Linares-Solano, A. *Carbon* **2004**, *42*, 1233–1242.
(45) Jagiello, J.; Thommes, M. *Carbon* **2004**, *42*, 1227–1232.
(46) Germain, J.; Svec, F.; Fréchet, J. M. J. *Chem. Mater.* **2008**, *20*, 7069–7076.
(47) Choi, J. H.; Choi, K. M.; Jeon, H. J.; Choi, Y. J.; Lee, Y.; Kang, J. K. *Macromolecules* **2010**, *43*, 5508–5511.
(48) Weber, J.; Schmidt, J.; Thomas, A.; Böhlmann, W. *Langmuir* **2010**, *26*, 15650–15656.
(49) Kowalczyk, P.; Hołyst, R.; Terzyk, A. P.; Gauden, P. A. *Langmuir* **2006**, *22*, 1970–1972.
(50) Kang, J.; Wei, S.; Kim, Y. *J. Am. Chem. Soc.* **2010**, *132*, 1510–1511.
(51) Tsujita, Y. *Prog. Polym. Sci.* **2003**, *28*, 1377–1401.
(52) Pandiyan, S.; Brown, D.; Neyertz, S.; van der Vegt, N. F. A. *Macromolecules* **2010**, *43*, 2605–2621.
(53) Chang, K.; Tung, C.; Wang, K.; Tung, K. *J. Phys. Chem. B* **2009**, *113*, 9821–9830.
(54) Bos, A.; Pünt, I. G. M.; Wessling, M.; Strathmann, H. *J. Membr. Sci.* **1999**, *155*, 67–78.
(55) Vishnyakov, A.; Ravikovitch, P. I.; Neimark, A. V. *Langmuir* **1999**, *15*, 8736–8742.
(56) Ravikovitch, P. I.; Vishnyakov, A.; Russo, R.; Neimark, A. V. *Langmuir* **2000**, *16*, 2311–2320.
(57) Yampolskii, Y. P. *Russ. Chem. Rev.* **2007**, *76*, 59–78.
(58) Stern, S. A.; Mi, Y.; Yamamoto, H.; Clair, A. K. S. *J. Polym. Sci., Part B: Polym. Phys.* **1989**, *27*, 1887–1909.
(59) Kochi, M.; Shimada, H.; Kambe, H. *J. Polym. Sci., Polym. Phys. Ed.* **1984**, *22*, 1979–1985.
(60) Shimazu, A.; Miyazaki, T.; Ikeda, K. *J. Membr. Sci.* **2000**, *166*, 113–118.
(61) The films were cut to fit into the sample tubes and should therefore have been opened to the outside.
(62) Wessling, M.; Huisman, I.; Boomgaard, T. V. D.; Smolders, C. A. *J. Polym. Sci., Part B: Polym. Phys.* **1995**, *33*, 1371–1384.
(63) Bas, C.; Tamagna, C.; Pascal, T.; Dominique Alberola, N. *Polym. Eng. Sci.* **2003**, *43*, 344–355.
(64) Liu, Q.; Mace, A.; Bacsik, Z.; Sun, J.; Laaksonen, A.; Hedin, N. *Chem. Commun.* **2010**, *46*, 4502–4504.